

Population dynamics method with a multi-canonical feedback control

Takahiro Nemoto,^{1,2} Freddy Bouchet,² Robert L. Jack,³ and Vivien Lecomte¹

¹*Laboratoire de Probabilités et Modèles Aléatoires, Sorbonne Paris Cité,
UMR 7599 CNRS, Université Paris Diderot, 75013 Paris, France*

²*Laboratoire de Physique, ENS de Lyon, Université de Lyon, CNRS, 46 allée d'Italie, 69364 Lyon, France*

³*Department of Physics, University of Bath, Bath BA2 7AY, United Kingdom*

(Dated: August 24, 2022)

We discuss the Giardinà-Kurchan-Peliti population dynamics method for evaluating large deviations of time averaged quantities in Markov processes [Phys. Rev. Lett. **96**, 120603 (2006)]. This method exhibits systematic errors which can be large in some circumstances, particularly for systems with weak noise, or close to dynamical phase transitions. We show how these errors can be mitigated by introducing control forces to within the algorithm. These forces are determined by an iteration-and-feedback scheme, inspired by multicanonical methods in equilibrium sampling. We demonstrate substantially improved results in a simple model and we discuss potential applications to more complex systems.

PACS numbers: 05.40.-a, 05.10.-a, 05.70.Ln

Introduction.— In many physical systems, interesting and important behaviour is associated with rare events – examples include crystal nucleation, slow transitions in biomolecules [1–3], rare transitions in turbulent flows [4, 5], and extreme events in climate dynamics [6]. Many computational methods for sampling these events have been proposed and exploited [1, 3, 5, 7–12]. One family of methods is based around population dynamics [13–18], in which several copies of a system evolve in parallel: the copies which exhibit the rare behaviour of interest are copied (or *cloned*) while other copies are discarded. The result is that *typical* copies within the population dynamics reproduce the desired rare events in the original system. One such method has recently been employed to characterise a particular class of rare events [7, 8], in which time-averaged physical quantities exhibit *large deviations* [19, 20] from their typical values in the large time limit. Studies of such events have revealed new and unexpected features in glass-formers [21], biomolecules [22–24], non-equilibrium transport [25, 26] and integrable systems [8]. In this article, we identify a pitfall that limits the computational efficiency of the population dynamics method, and we show it can be modified so as to avoid this problem. The issue at stake is the number of copies of the system that must be considered in order to obtain accurate results – if very many copies are required then the method is difficult to apply, especially if even a single system is complex or contains many degrees of freedom. In some relevant cases then the standard population dynamics method requires an exponentially large population to be effective [27]. However, the method that we propose here, which is inspired by multicanonical methods in equilibrium systems [28, 29], can still be effective in these cases. We argue that this new method will provide a step-change in the complexity of the systems for which large deviation computations can be performed.

Rare event problem— The rare events that we consider can take place in a variety of models. To illustrate the method, consider a particle moving in d -dimensions, whose position $x \in \mathbf{R}^d$ obeys a Langevin equation

$$\dot{x}_t = F(x_t) + B(x_t)\xi_t, \quad (1)$$

where ξ is a d -dimensional Gaussian white noise of unit variance, $F(x) \in \mathbf{R}^d$ a deterministic force, and $B(x)$ a $d \times d$ matrix specifying the action of the noise on the particle [30]. We use the Itô convention [31] for stochastic calculus throughout this paper.

We restrict to ergodic systems, and we focus on rare events in which a time averaged quantity $\Lambda(\tau)$ takes some non-typical value. Here τ is the long time period over which the average is taken, and $\Lambda(\tau) = \Lambda_d(\tau) + \Lambda_c(\tau)$ consists of a configurational contribution $\Lambda_d(\tau) = \frac{1}{\tau} \int_0^\tau \lambda_d(x_t) dt$ and a current one $\Lambda_c(\tau) = \frac{1}{\tau} \int_0^\tau \lambda_c(x_t) \cdot dx_t$, where $\lambda_{d,c}$ are arbitrary functions of the particle position x . Typical examples of Λ are entropy production [32, 33], dynamical activity [21, 34], and particle fluxes [35].

In the limit of large τ , ergodicity of the system means that the observable $\Lambda(\tau)$ is almost surely equal to its typical value $\bar{\Lambda}$. Our aims are (i) to estimate the (small) probability of deviations from this value, and (ii) to generate the rare trajectories that lead to these deviations. This is an important problem because these non-typical trajectories can exhibit interesting and unusual structures, including misfolded proteins [23, 24], stable glass states [21] and travelling waves in models of particle transport [25].

To achieve these aims, the standard theoretical route [19, 32] is to introduce a *biasing field* h , which controls deviations of $\Lambda(\tau)$ from its typical value. Specifically, we consider an ensemble of paths $X = (x_t)_{t=0}^\tau$ with (unnormalised) probability density $P_h[X] = \pi_0(x_0) \exp \left[- \int_0^\tau \mathcal{L}(x_t, \dot{x}_t) dt + h\tau\Lambda(\tau) \right]$, where

$$\mathcal{L}(x, \dot{x}) = \frac{1}{2} [\dot{x} - F(x)] \cdot \kappa(x)^{-1} [\dot{x} - F(x)] \quad (2)$$

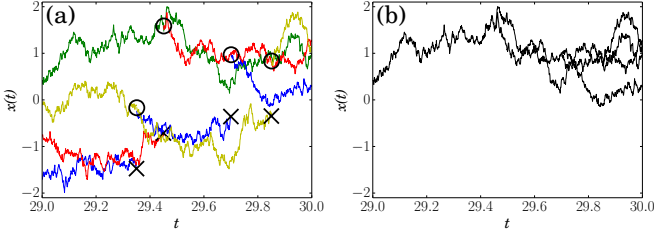


FIG. 1. (a) Trajectories $x^a(t)$ generated by population dynamics at fixed total population $N_c = 4$ for the model system described in the main text ($\epsilon = 1, h = 1$). At certain times, some copies of the system are removed (\times) and others are duplicated (\circ). (b) Representative sample paths $\tilde{x}_a(t)$ for the distribution $P_h[X]$, derived from those in (a) by keeping only trajectories surviving up to final time $\tau = 30$.

is a Lagrangian density that describes the (unbiased) model (1); $\pi_0(x)$ is the initial condition for the trajectories, that can be arbitrary and which we take to be the stationary probability distribution of the unbiased model in the numerical examples. Also, $\kappa = BB^T$ where the notation B^T indicates a matrix transpose [36].

Normalised averages with respect to P_h are denoted by $\langle \cdot \rangle_h$ and we use these averages to characterise the rare trajectories associated with deviations of $\Lambda(\tau)$ from $\bar{\Lambda}$, for the model in Eq. (1). We define the scaled cumulant generating function (CGF): $G(h) = \lim_{\tau \rightarrow \infty} \tau^{-1} \log \langle e^{th\Lambda(\tau)} \rangle_0$. In the limit of large τ , the probability distribution of $\Lambda(\tau)$ satisfies a large deviation principle, and can be obtained by a Legendre transformation of $G(h)$ [19, 20]. In the same limit, for a given deviation Λ from $\bar{\Lambda}$, there exists a bias $h^*(\Lambda)$ for which $\langle \cdot \rangle_{h^*(\Lambda)}$ is equivalent to a conditional average over trajectories with $\Lambda(\tau) = \Lambda$ [37].

Population dynamics method – There are several computational methods that allow evaluation of averages with respect to P_h [7, 11, 12, 38]. In the population dynamics method [7], one considers N_c copies (or clones) of the system. These clones evolve independently as a function of the time t , except that (for $h > 0$) clones with small $\Lambda(t)$ are periodically removed from the system, while clones with large $\Lambda(t)$ are duplicated, to maintain a constant population. The algorithm is described fully in Supplemental Material (SM) [39]. This method biases the system towards the rare events of interest. For sufficiently large N_c (and large enough τ), the method provides accurate estimates of $G(h)$ and it generates sample paths consistent with the biased distribution P_h .

The operation of the method is illustrated in Fig. 1 for a one-dimensional model of a particle in a quartic potential. Fig. 1(a) shows four copies of the system that evolve in time, except that some trajectory segments stop and others branch, as the cloning operates. Fig. 1(b) shows four representative trajectories (sample paths) for the distribution $P_h[X]$, which have been reconstructed from panel (a), by tracing backwards in time from the

clones that survived up to the final time τ .

Sampling errors within population dynamics – The accuracy of the population dynamics is limited by issues originating from clone multiplicity, as we now explain. Consider the distribution

$$p_{\text{ave}}(x) = \lim_{\tau \rightarrow \infty} \left\langle \tau^{-1} \int_0^\tau \delta(x_t - x) dt \right\rangle_h, \quad (3)$$

which indicates the fraction of time spent at position x , within the biased ensemble. We also define

$$p_{\text{end}}(x) = \lim_{\tau \rightarrow \infty} \langle \delta(x_\tau - x) \rangle_h, \quad (4)$$

which indicates the fraction of trajectories for which the particle's final position is x . For the stationary state of the dynamics (1), which corresponds to $h = 0$, time-translational invariance ensures that $p_{\text{ave}} = p_{\text{end}}$. However, this is not the case for biased ensembles where $h \neq 0$, as illustrated in [7, 40].

The population dynamics method provides estimates of both p_{ave} and p_{end} . Let the position of clone a at time t be $x^a(t)$, with $a = 1 \dots N_c$. Recalling Fig. 1(a), note that the functions $x^a(t)$ are not continuous in time and do not represent sample paths for the distribution $P_h[X]$. To construct sample paths, which we denote by $\tilde{x}^a(t)$, we trace backwards in time from the clones that survive up to τ , as shown in Fig. 1(b). There are still N_c paths \tilde{x}^a , but these overlap, particularly at early times. The multiplicity $m_a(t)$ of $\tilde{x}^a(t)$ is the number of its descendants at the final time τ . With these definitions, one arrives at statistical estimators for distributions: $p_{\text{end}}(x) \approx (1/N_c) \sum_{a=1}^{N_c} \delta(x - x^a(t))$, and $p_{\text{ave}}(x) \approx (1/N_c) \sum_{a=1}^{N_c} \delta(x - \tilde{x}^a(t))$ in their stationary regime [39]. These approximate equalities become exact in the limit $N_c \rightarrow \infty$, in which the population dynamics gives exact results.

From the estimators of p_{ave} and p_{end} provided above, one sees that the typical multiplicity of a clone with position x is $p_{\text{ave}}(x)/p_{\text{end}}(x)$. If this ratio is large, then the population dynamics requires many clones, in order to obtain accurate results. To see this, define $x^* = \arg \max_x [p_{\text{ave}}(x)]$ as the most likely value of x , within the distribution p_{ave} . The population dynamics requires that the typical multiplicity of a clone with position x^* should be of order $m^* = p_{\text{ave}}(x^*)/p_{\text{end}}(x^*)$. This clearly cannot be achieved unless $N_c \gtrsim m^*$, which provides an estimate of the number of clones required for accurate results. If this condition is not satisfied, the population dynamics algorithm suffers from large *systematic errors*, which cannot be eliminated by merely running the algorithm several times. We also note that if typical clone multiplicities m_a are large, the number of *independent* clones within the population is suppressed by a factor of order m_a , which leads to large *statistical (random) errors* in the algorithm.

Controlled dynamics – To resolve this problem, we introduce a “control strategy”, which modifies the original

model (1), in order to make the rare events of interest more likely. (These large deviation problems have dual representations in terms of optimal control problems [41–45], which provide a natural interpretation of the method presented here.) The modified model is

$$\dot{x}_t = F(x_t) + w(x_t) + B(x_t)\xi_t, \quad (5)$$

where $w(x)$ is a controlling force which we write as $w(x) = h\kappa\lambda_c(x) - \kappa\nabla V(x)$, where V acts as a potential. Then [39], averages with respect to the biased distribution P_h can be rewritten as averages with respect to this modified dynamics, but with a bias on a different observable Λ^w , which replaces Λ . That is,

$$P_h[X] = P_w[X]e^{V(x_\tau) - V(x_0)} \quad (6)$$

with $P_w[X] = \pi_0(x_0) \exp \left[-\int_0^\tau \mathcal{L}^w(x_t, \dot{x}_t) dt + h\tau\Lambda^w(\tau) \right]$, where \mathcal{L}^w is obtained by replacing $F \mapsto F + w$ in (2). Also $\Lambda^w = \frac{1}{\tau} \int_0^\tau \lambda^w(x_t) dt$, with $\lambda^w = \lambda_d + \frac{1}{h}[(F + w/2) \cdot \kappa^{-1}w - \frac{1}{2}\text{Tr}(H_V\kappa)]$, where H_V is a Hessian matrix with elements $(\partial^2 V / \partial x_i \partial x_j)$.

Averages with respect to P_w are denoted by $\langle \cdot \rangle_w$, and can be calculated using the population dynamics method with the modified model (5). Physically, (6) says that rare events for the system (1) have an alternative characterisation as rare events for the controlled system (5). More precisely, from (6), the averages $\langle \cdot \rangle_h$ and $\langle \cdot \rangle_w$ are not equal, but their associated probability distributions differ only through boundary terms at initial and final times. For large τ , we focus on properties far from initial and final times, in which case the averages $\langle \cdot \rangle_h$ and $\langle \cdot \rangle_w$ are equivalent. This equivalence implies that $p_{\text{ave}} = p_{\text{ave}}^w$, where p_{ave}^w is defined as in (3) but for the controlled population dynamics. On the other hand, the end-time distribution p_{end}^w for the controlled dynamics differs from its uncontrolled counterpart as $p_{\text{end}}^w \propto p_{\text{end}} e^{-V(x)}$, as read from (6) [39]. Thus the control w allows p_{end}^w to be varied, while always keeping p_{ave}^w constant.

Optimal control – These results apply for any control force w , but a (unique) optimal choice w^* can be defined by the condition $p_{\text{ave}}^{w^*} = p_{\text{end}}^{w^*}$. This choice implies that $\lambda^w(x)$ is independent of x [39], so that there is no cloning or deletion of clones in the resulting population dynamics algorithm. The optimally-controlled process [41–45] generates directly the path measure P_h , up to the corrections given in (6) [46–50].

Iteration and feedback – Based on these results we now introduce an iterative strategy for solving the original rare event problem (see [12] for a similar idea). Starting with some (non-optimal) control w , and its corresponding potential V , we use population dynamics to generate sample paths from P_w . From the definition of the optimal force ($p_{\text{end}}^{w^*} = p_{\text{ave}}^{w^*}$) and the relations between $p_{\text{end,ave}}^w$ and $p_{\text{end,ave}}$, we obtain

$$\frac{p_{\text{end}}^w(x)}{p_{\text{ave}}^w(x)} e^{V(x)} = e^{V^*(x)} \quad (7)$$

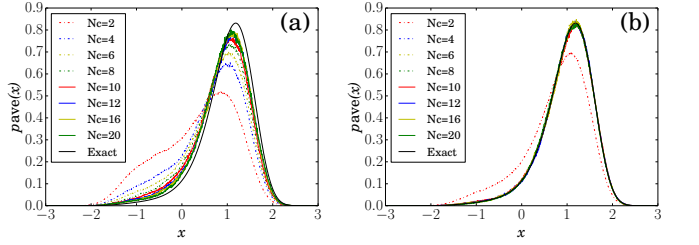


FIG. 2. Distributions $p_{\text{ave}}(x)$ for the simple model described in the text, calculated (a) from the standard population dynamics method and (b) from the controlled population dynamics with iteration-and-feedback. We take $\epsilon = 1$ and $h = 1$, with a various different numbers of clones N_c . The exact distribution $p_{\text{ave}}(x)$ is shown as a black line. The convergence with respect to N_c is improved significantly by the iteration-and-feedback method.

where V^* is the potential V corresponding to the optimal control w^* . Since all terms on the left-hand side of (7) can be measured from the population dynamics, this allows an estimate of V^* , and hence of w^* . The population dynamics calculation is then repeated, using this estimated w^* as the new control w [39]. On iteration of this scheme, one expects that V approaches V^* , so Eq. (7) means that p_{end}^w converges to p_{ave}^w . Thus, in the population dynamics, the typical clone multiplicities $m_a(t)$ decrease as the method is iterated, improving the sampling problems discussed above. This method, which generates sample paths from P_h , is similar to multicanonical methods such as Wang-Landau sampling [29] which generate sample configurations from equilibrium distributions.

Numerical example.—We apply this method to a model of diffusion in a quartic potential, as introduced in Fig. 1. That is, $F(x) = -x^3$ and $B(x) = \sqrt{2\epsilon}$, where ϵ is the noise strength (or temperature). We take $\lambda_c = 0$ and $\lambda_d = x(x+1)$. For $h < 0$ the distribution P_h is concentrated on trajectories with small values of λ_d , which tend to localise near $x \approx -\frac{1}{2}$. Here we focus on the case $h > 0$, which leads to unusually large values of λ_d . Those can be realised either for $x > 0$ or $x < 0$ but at large τ this rare event is almost always realised by trajectories that have $x > 0$, as in Fig. 1. This simple problem can be solved exactly in the zero-noise limit [39].

To implement the iteration-and-feedback method, we parameterise the control potential as a quartic polynomial $V(x) = c_1x + c_2x^2 + c_3x^3 + c_4x^4$. For the first iteration of the method we take $V = 0$. Fig. 2 shows estimates of the distribution p_{ave} obtained using the original cloning method, compared with the results obtained using three iterations of the control-with-feedback procedure proposed here, for $h = 1$, $\epsilon = 1$ and $\tau = 36000/N_c$. We decrease τ with increasing N_c so we work at fixed computational cost [51]. Fig. 2 shows that the number of clones required to obtain convergence to the exact result is much reduced using the cloning-with-control method.

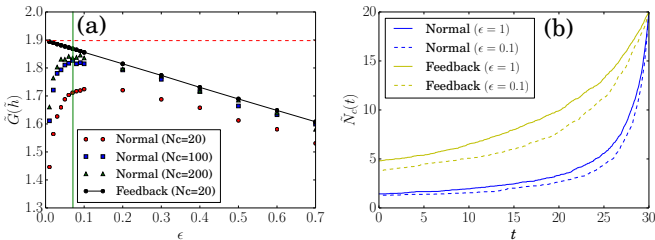


FIG. 3. (a) Estimates of $\tilde{G}(\tilde{h} = 1)$, as ϵ is varied. We compare results from the normal population dynamics and from the control-with-feedback method. The analytical result for $\lim_{\epsilon \rightarrow 0} \tilde{G}(\tilde{h})$ is shown as a dashed line. The standard method fails at small ϵ but the control-with-feedback method converges to the correct value. (b) Number of distinct clones $\tilde{N}_c(t)$, comparing the standard and the controlled population dynamics. The larger values of $\tilde{N}_c(t)$ obtained with the control-with-feedback method lead to smaller statistical uncertainties in the results.

In the weak-noise limit $\epsilon \rightarrow 0$, one can see this advantage more clearly. In this limit, it is natural to consider a rescaled cumulant generating function $\tilde{G}(\tilde{h}) \equiv \epsilon G(h)$ with $\tilde{h} \equiv h\epsilon$ [52]. Fig. 3(a) shows numerical results for this function, as ϵ is reduced. The normal population dynamics converges very poorly below a certain value of ϵ . (The green vertical line shows the value ϵ for which $p_{\text{end}}(x^*) \sim e^{-1}$ [53]). However, the controlled population dynamics does not fail at small ϵ because it maintains $p_{\text{end}}^w \approx p_{\text{ave}}^w$ [54].

Finally, we consider *statistical* errors. Fig. 3(b) shows the number of distinct clone positions in the population, $\tilde{N}_c(t)$. Again, the cloning-with-control method performs better than the original method, in that it averages over a larger sample of distinct positions, reducing the statistical errors. The method yields the function $G(h)$, which specifies the probabilities of rare events; it also generates sample paths from $P_h(X)$. Finally, the optimal control provides a simple *physical* strategy for promoting the rare events of interest in this illustrative model system.

Outlook – We have shown that the performance of the population dynamics algorithm for sampling large deviations [7] can be improved by introducing a controlling force w . Given the optimal choice for this force, the rare events of interest in large deviation theory can be characterised as typical trajectories of the controlled system. In complex systems with many degrees of freedom it is likely that the optimal w cannot be determined exactly, but even non-optimal controls can still significantly improve both the statistical and the systematic errors associated with the population dynamics method. (Note that the results of Fig. 3 used a quartic approximation to V which do not perfectly capture the optimal control V^* [39].) It is straightforward to improve existing population dynamics codes to include this approach: we expect that it will significantly expand the range of systems for which numerical calculations can be performed,

including open quantum systems [55, 56], or more complex molecular dynamics models than those considered so far [21, 57].

The authors are grateful for support Fondation Sciences Mathématiques de Paris – EOTP NEMOT15RPO, PEPS LABS and LAABS Inphyniti CNRS project. The research leading to these results has received funding from the European Research Council under the European Union’s seventh Framework Programme (FP7/2007-2013 Grant Agreement No. 616811) (F. Bouchet and T. Nemoto)

- [1] S. Auer and D. Frenkel, *Nature* **409**, 6823 (2001).
- [2] R. P. Sear, *J. Phys.: Cond. Matt.* **19**, 033101(2007).
- [3] W. Ren, E. Vanden-Eijnden, P. Maragakis and W. E, *J. Chem. Phys.* **123**, 134109 (2005).
- [4] M. Berhanu, *et al.*, *Europhys. Lett.* **77**, 59001 (2007).
- [5] F. Bouchet, and E. Simonnet, *Phys. Rev. Lett.* **102**, 094504 (2009).
- [6] D. R. Easterling, G. A. Meehl, C. Parmesan, S. A. Changnon, T. R. Karl, L. O. Mearns, *Science*, **289**, 2068 (2000).
- [7] C. Giardinà, J. Kurchan, and L. Peliti, *Phys. Rev. Lett.* **96**, 120603 (2006).
- [8] J. Tailleur, and J. Kurchan, *Nature Physics*, **3**, 203 (2007).
- [9] P. L. Ecuyer, V. Demers, and B. Tuffin, *Proceedings of the 2006 Winter Simulation Conference*, 137, (2006).
- [10] R. J. Allen, P. B. Warren, and P. R. ten Wolde, *Phys. Rev. Lett.* **94**, 018104 (2005).
- [11] P. G. Bolhuis, D. Chandler, C. Dellago, and P. L. Geissler, *Annu. Rev. Phys. Chem.* **53**, 291 (2002).
- [12] T. Nemoto and S.-i. Sasa, *Phys. Rev. Lett.* **112**, 090602 (2014).
- [13] J. B. Anderson, *J. Chem. Phys.* **63**, 1499 (1975).
- [14] D. Aldous and U. Vazirani, in *Proc. 35th IEEE Sympo. on Foundations of Computer Science* (1994).
- [15] P. Grassberger, *Comp. Phys. Comm.* **147** 64 (2002).
- [16] P. Del Moral, and J. Garnier, *The Annals of Applied Probability*, **15**, 2496 (2005).
- [17] F. Cérou, A. Guyader, T. Lelièvre and D. Pommier, *J. Chem. Phys.* **134** 054108 (2011).
- [18] J. Rolland, F. Bouchet and E. Simonnet, *J. Stat. Phys.* **162**, 277 (2016).
- [19] H. Touchette, *Phys. Rep.* **478**, 1, (2009).
- [20] A. Dembo and O. Zeitouni, *Large deviations techniques and applications* (Springer, New York, 1998).
- [21] L. O. Hedges, R. L. Jack, J. P. Garrahan and D. Chandler, *Science* **323** 1309 (2009).
- [22] M. Picciani, M. Athènes, J. Kurchan and J. Tailleur, *J. Chem. Phys.* **135** 034108 (2011).
- [23] J. K. Weber, R. L. Jack and V. S. Pande, *J. Am. Chem. Soc.* **135**, 5501 (2013).
- [24] A. S. J. S. Mey, P. L. Geissler and J. P. Garrahan, *Phys. Rev. E* **89**, 032109 (2014).
- [25] P. I. Hurtado, C. P. Espigares, J. J. del Pozo, P. L. Garrido, *J. Stat. Phys.* **154**, 214 (2014).
- [26] B. Derrida, *J. Stat. Mech.* 2007, P07023 (2007).
- [27] P. I. Hurtado and P. L. Garrido, *J. Stat. Mech.* (2009)

[28] B. A. Berg and T. Neuhaus, Physics Letters B **267**, 249 (1991).

[29] F. Wang and D.P. Landau, Phys. Rev. Lett. **86**, 2050 (2001).

[30] All the results presented here can be generalised to models with n interacting particles, by replacing $d \rightarrow nd$ and including interaction forces in $F(x)$. Markov jump processes are also workable.

[31] C. W. Gardiner, *Handbook of Stochastic Methods for Physics, Chemistry, and the Natural Sciences* (Springer-Verlag, Berlin, 1983).

[32] J. L. Lebowitz and H. Spohn, J. Stat. Phys. **95**, 333 (1999).

[33] V. Lecomte, C. Appert-Rolland and F. van Wijland, J. Stat. Phys. **127**, 51 (2007).

[34] J. P. Garrahan, R. L. Jack, V. Lecomte, E. Pitard, K. van Duijvendijk and F. van Wijland, Phys. Rev. Lett. **98**, 195702 (2007).

[35] T. Bodineau and B. Derrida, Phys. Rev. E **72**, 066110 (2005).

[36] The matrix κ is assumed to be invertible but the generalization to non-invertible κ is direct.

[37] H. Touchette, J. Stat. Phys. **159**, 987 (2015).

[38] V. Lecomte and J. Tailleur, J. Stat. Mech. (2007) P03004.

[39] See Supplemental Material.

[40] J. P. Garrahan, R. L. Jack, V. Lecomte, E. Pitard, K. van Duijvendijk, and F. van Wijland, J. Phys. A **42**, 075007 (2009).

[41] R. L. Jack and P. Sollich, Eur. Phys. J: Special Topics **224**, 2351 (2015).

[42] R. Chetrite and H. Touchette, J. Stat. Mech. **2015** P12001, (2015).

[43] W. H. Fleming, *Stochastic control and large deviations*, in *Future Tendencies in Computer Science, Control and Applied Mathematics*, pages 291-300 (Springer, Berlin, 1992).

[44] C. Hartmann and C. Schütte, J. Stat. Mech. (2012), P11004

[45] V. Y. Chernyak, M. Chertkov, J. Bierkens and H. J. Kappen, J. Phys. A **47**, 022001 (2013).

[46] R. M. L. Evans, Phys. Rev. Lett. **92**, 150601 (2004).

[47] R. L. Jack and P. Sollich, Prog. Theor. Phys. Suppl. **184**, 304 (2010).

[48] T. Nemoto and S.-i. Sasa, Phys. Rev. E **84**, 061113 (2011).

[49] C. Maes and K. Netocny, EPL **82**, 30003 (2008).

[50] R. Chetrite and H. Touchette, Ann. Henri Poincaré **16**, 2005, (2015).

[51] More precisely, we divide this time interval τ into several bins, where each of which is sufficiently large to obtain p_{ave} . The estimated p_{ave} is the average of them. See [39] for the detail.

[52] In the weak-noise limit $\epsilon \rightarrow 0$, the dynamics of the system runs increasingly slowly so it is necessary to rescale either the time variable or (equivalently) the biasing field h like this. Indeed, this scaled CGF, and also p_{end} , p_{ave} , have a well-defined limit as $\epsilon \rightarrow 0$ (at fixed \tilde{h}). The function \tilde{G} is singular at $\tilde{h} = 0$, indicating a dynamical phase transition [39].

[53] This condition is (roughly) equivalent to the relation $N_c \sim m^*$ that is used for accuracy-criterion of the population dynamics method (See paragraph *Sampling errors within population dynamics*).

[54] The numerical calculations exploit an “annealing procedure” in which ϵ is reduced in steps of size $\delta\epsilon = 0.01$, with the best estimate of w^* from the each step being used as the first guess for w^* in the subsequent step.

[55] Juan P. Garrahan and Igor Lesanovsky, Phys. Rev. Lett. **104**, 160601 (2010).

[56] James M. Hickey, Sam Genway, Igor Lesanovsky, and Juan P. Garrahan Phys. Rev. A **86**, 063824 (2012).

[57] T. Speck, A. Malins and C. P. Royall, Phys. Rev. Lett. **109**, 195703 (2012).

Supplemental material for “Population dynamics method with a multi-canonical feedback control”

Takahiro Nemoto,^{1,2} Freddy Bouchet,² Robert L. Jack,³ and Vivien Lecomte¹

¹*Laboratoire de Probabilités et Modèles Aléatoires, Sorbonne Paris Cité,
UMR 7599 CNRS, Université Paris Diderot, 75013 Paris, France*

²*Laboratoire de Physique, ENS de Lyon, Université de Lyon, CNRS, 46 allée d’Italie, 69364 Lyon, France*

³*Department of Physics, University of Bath, Bath BA2 7AY, United Kingdom*
(Dated: January 25, 2016)

These are supplemental materials for the paper “Population dynamics method with a multi-canonical feedback control”. The materials are divided into four sections.

PACS numbers: 05.40.-a, 05.10.-a, 05.70.Ln

Contents

I. Population dynamics method	1
A. Algorithm	1
B. Generating continuous sample paths for the biased dynamics	2
C. Numerical example	3
II. Derivation of the ratio of path probability density (6)	3
A. Derivation using path probability density	3
B. Derivation using time-evolution operator	4
III. An algorithm for population dynamics with a feedback control	6
IV. Langevin system with quartic potential	7
A. Euler-Lagrange equation (Instanton equation)	8
B. Steady solutions	9
C. Cumulant generating function	9
D. Analytical expressions of $p_{\text{end}}(x)$ and $p_{\text{ave}}(x)$ in $\epsilon \rightarrow 0$	9
References	11

I. POPULATION DYNAMICS METHOD

In this section, complementing the sections *Population dynamics method* and *Sampling errors within population dynamics* in the main text, we explain the details of the population dynamics algorithm. We demonstrate that for large numbers of clones, it converges to the correct results for the simple model discussed in the main text.

A. Algorithm

The population dynamics is a numerical technique designed to evaluate a large deviation function associated to the cumulant generating function (CGF) of a time-averaged observable $\Lambda(t)$. The algorithm is constituted of a normal dynamics sequence, and an elimination-multiplication sequence that is performed at periodic times separated by an interval ΔT :

1. Generate N_c initial conditions, for example, drawn from the stationary state of the original ($h = 0$) dynamics.
2. Repeat the following procedure M times. (m is the iteration index representing how many times the procedure is repeated up to m .)

(a) Perform the normal dynamics from $t = m \Delta T$ to $(m + 1)\Delta T$. We denote each trajectory by $x^a(t)$ ($a = 1, 2, \dots, N_c$). During the simulation, for each realisation, calculate

$$s_a = \exp \left\{ h [(t + \Delta T) \Lambda(t + \Delta T) - t \Lambda(t)] \right\}. \quad (\text{S1})$$

(b) After the simulation of the time interval ΔT , for each trajectory, define an integer number n_a ($a = 1, 2, \dots, N_c$) by

$$n_a = \left\lfloor \frac{s_a}{\sum_b s_b} N_c + \eta \right\rfloor, \quad (\text{S2})$$

where η is a random number uniformly distributed on $[0,1]$ and $\lfloor \cdot \rfloor$ denotes the lower integer part. Then, multiply or eliminate each trajectory according to this number. (E.g. $n_a = 0$ means that we kill the trajectory a . $n_a = 5$ means that we prepare 4 other copies of the trajectory a .) If, after this operation, the total number of trajectories is not equal to N_c , we eliminate or multiply enough copies, chosen randomly and uniformly, in order to make the total number of trajectories to be N_c .

(c) At the same time, store the value of $\sum_b s_b$ and denote it by S_m .
(d) The new ensemble is used as the initial condition of the next time interval.

Finally, the CGF [7] and p_{end} are evaluated as

$$G(h) \sim \frac{1}{M \Delta T} \sum_m \log S_m. \quad (\text{S3})$$

and

$$\int f(x) p_{\text{end}}(x) dx \simeq \frac{1}{N_c} \sum_{a=1}^{N_c} f(x^a(\tau)), \quad (\text{S4})$$

where these formulas are directly obtained from their definitions. For the latter equality, we note that we can improve the statistics by using the history of $x_a(t)$. More precisely, by assuming an “ergodicity property”, we replace $f(x^a(\tau))$ by the corresponding time-average from $t = 0$ to $t = \tau$: $(1/\tau) \int_0^\tau f(x^a(t)) dt$. This improved expression is

$$\int f(x) p_{\text{end}}(x) dx \simeq \frac{1}{\tau N_c} \sum_{a=1}^{N_c} \int_0^\tau f(x^a(t)) dt, \quad (\text{S5})$$

which means that p_{end} is expressed as the time averaged value (or the stationary value) of empirical distribution of $x_a(t)$ as announced in the section: *Sampling errors within population dynamics* of the main text.

B. Generating continuous sample paths for the biased dynamics

To complete the description of the population dynamics method, we describe the construction of the continuous sample paths $\tilde{x}(t)$ described in the main text. If we do not require full sample paths but only wish to evaluate the biased average of an additive observable $A(\tau) = \int_0^\tau a(x(t)) dt$, a simple method [S1] consists in attaching a value of the observable A to every trajectory and, at every time step, to update its value and copy/delete it together with the trajectory. Then, an evaluation of the biased average of A is given by the average of the numerical values of A attached to every trajectory present at final time.

To obtain full sample paths (and hence distributions such as p_{ave}) we analyse the trajectories that survive in the population dynamics up to time τ , and reconstitute the paths backwards in time. The procedure is as follows: we first generate the trajectories and then perform a selection of the trajectories based on the conditioning of survival up to the final time τ . Considering the N_c copies at final time, indexed by $1 \leq a \leq N_c$, one can follow the ancestors of every copy. Upon every coalescence observed backwards in time (corresponding to multiplications of clones in the original forwards simulation), one increments a counter $m_a(t)$ by the number of trajectories which have coalesced. At the end of the procedure, the counters $(m_a(t))_{1 \leq a \leq N_c}$ represent, at time t , the number of descendants of a copy a at final time τ . To avoid multiple counting, one can select at every coalescence a particular branch, and keep track of $\tilde{N}_c(t)$ ($1 \leq \tilde{N}_c(t) \leq N$) indices of independent (or distinct) trajectories instead. In these indices, by an appropriate

reindexing, one can define the independent sequence of their multiplicities $(k_{\tilde{a}}(t))_{1 \leq \tilde{a} \leq \tilde{N}_c(t)}$ and trajectories $(y^{\tilde{a}}(t))$ ($\tilde{a} = 1, 2, \dots, \tilde{N}_c(t)$). For example, by defining $K_{\tilde{a}} = \sum_{b=1}^{\tilde{a}-1} k_b$, one has

$$y^{\tilde{a}}(t) \equiv \tilde{x}^{K_{\tilde{a}}+1}(t) = \dots = \tilde{x}^{K_{\tilde{a}}+k_{\tilde{a}}}(t) \quad (\text{S6})$$

$$k_{\tilde{a}} \equiv m_{K_{\tilde{a}}+1} = \dots = m_{K_{\tilde{a}}+k_{\tilde{a}}} \quad (\text{S7})$$

for $\tilde{a} = 1, 2, \dots, \tilde{N}_c(t)$, and where the $(\tilde{x}^a(t))_{1 \leq a \leq N_c}$ are the trajectories used in the main text. By using these trajectories, p_{ave} is calculated as

$$\int f(x)p_{\text{ave}}(x)dx \simeq \frac{1}{\tau N_c} \int_0^\tau \sum_{\tilde{a}=1}^{\tilde{N}_c(t)} k_{\tilde{a}}(t) f(y^{\tilde{a}}(t)) dt. \quad (\text{S8})$$

This means that p_{ave} is calculated as the time-averaged value (or the stationary value) of the empirical distribution of \tilde{x}^a , as announced in the section: *Sampling errors within population dynamics* of the main text [8].

C. Numerical example

To verify the accuracy of this method, we consider a particle moving in a quartic potential as described in the main text. (That is, $d = 1$, $F(x) = -x^3$, $B(x) = \sqrt{\epsilon}$, $\lambda_d(x) = \lambda(x) \equiv x^2 + x$, and $\lambda_c(x) = 0$.) We estimate p_{ave} and p_{end} from this method and show them in Fig.S1. In the same figure, we also plot the numerically exact distributions, obtained by numerical solution of a modified Fokker-Planck equation (see [S2] and Section II B below). The population dynamics converges to the exact result as N_c is increased.

We also show the (continuous) trajectories $(y^{\tilde{a}}(t))$ ($\tilde{a} = 1, 2, \dots, \tilde{N}_c(t)$) generated with this method in Fig.S2.(b) and the numerical evaluation of $\tilde{N}_c(t)$ in Fig.S3. We note that the independent number of copies $\tilde{N}_c(t)$ decreases as t decreases to 0.

II. DERIVATION OF THE RATIO OF PATH PROBABILITY DENSITY (6)

In this section, complementing the sections *Controlled dynamics* and *Optimal control* in the main text, we derive the relation between $P_h[X]$ and $P_w[X]$ [eq.(6) in the main text]. We show the derivation in two ways, one based on path probability densities (stochastic differential equations) and the other on Fokker-Planck equations.

A. Derivation using path probability density

We denote by $X = (x(t))_{0 \leq t \leq \tau}$ the trajectories. From the definitions of $P_h[X]$ and $P_w[X]$, we have

$$\frac{P_w[X]e^{-h\tau\Lambda^w(\tau)}}{P_h[X]e^{-h\tau\Lambda(\tau)}} = \exp \left[\int_0^\tau (\dot{x} - F) \cdot \kappa^{-1} w dt - \frac{1}{2} \int_0^\tau w \cdot \kappa^{-1} w dt \right] \quad (\text{S9})$$

The integrand on the right-hand side is written as

$$(\dot{x} - F) \cdot \kappa^{-1} w - \frac{1}{2} w \cdot \kappa^{-1} w = \dot{x} \cdot (-\nabla V + h\lambda_c) - \left(F + \frac{1}{2} w \right) \cdot \kappa^{-1} w, \quad (\text{S10})$$

where we have used the expression of $w(x)$ as given in the main text ($w(x) = \kappa[-\nabla V(x) + h\lambda_c(x)]$). We then consider the integral of the first term on the right hand side:

$$\int_0^\tau \dot{x} \cdot (-\nabla V) dt. \quad (\text{S11})$$

Since the trajectory X is generated from the stochastic differential equation (5) and we use the Itô convention, the time-derivative of $V(x(t))$ is given by Itô's formula

$$\frac{d}{dt} V = \dot{x} \cdot \nabla V + \frac{1}{2} \text{Tr} [B^T H_V B]. \quad (\text{S12})$$

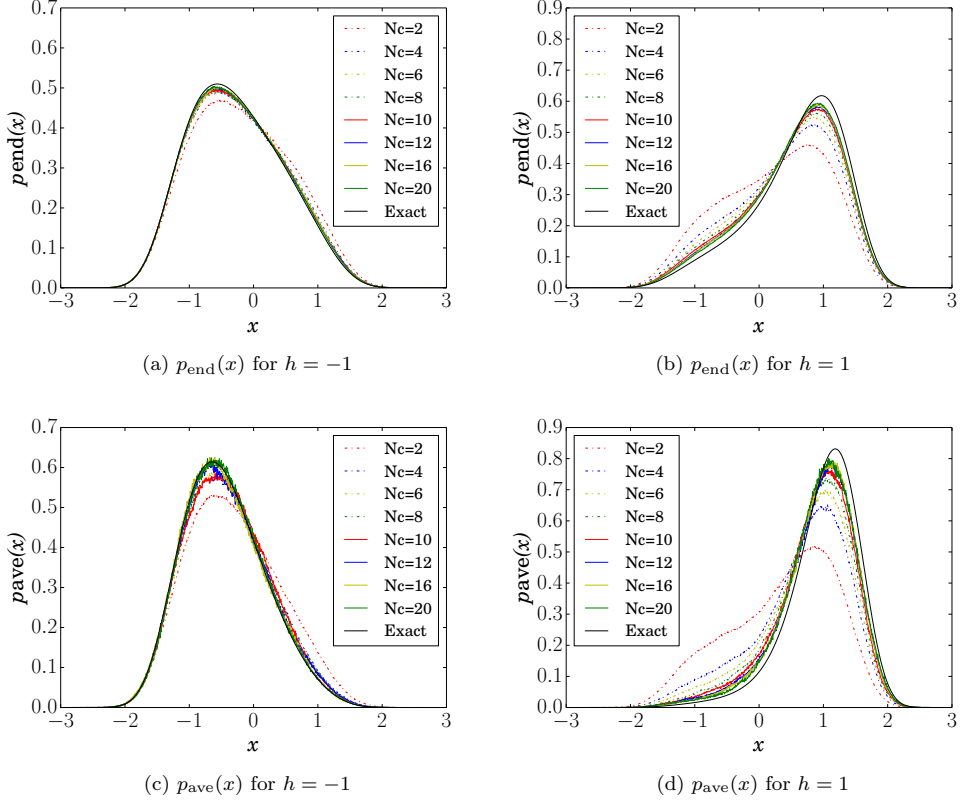


FIG. S1: (a), (b) $p_{\text{end}}(x)$ calculated from population dynamics method. The numerically exact result is plotted as a black line. (c), (d) $p_{\text{ave}}(x)$ calculated from the population dynamics method, together with the numerically exact result. We set $\epsilon = 1$ for time interval $\tau = 30$. We repeat the simulation $1200/N_c$ times and the result is the average of them. We can see the convergence of the results of population dynamics to the analytical ones.

Here H_V is a Hessian matrix defined as $(H_V)_{i,j} = \frac{\partial V}{\partial x_i \partial x_j}$. From (S12), (S11) becomes

$$\int_0^\tau \dot{x} \cdot (-\nabla V) dt = -V(x(\tau)) + V(x(0)) + \int_0^\tau \frac{1}{2} \text{Tr} [B^T H_V B] dt. \quad (\text{S13})$$

Thus, from (S9), (S10) and (S13), we get

$$\frac{P_w[X] e^{-h\tau\Lambda^w(\tau)}}{P_h[X] e^{-h\tau\Lambda(\tau)}} = e^{-V(x(\tau)) + V(x(0))} \exp \left\{ \int_0^\tau \left[\frac{1}{2} \text{Tr} [B^T H_V B] + h\dot{x} \cdot \lambda_c - \left(F + \frac{w}{2} \right) \cdot \kappa^{-1} w \right] dt \right\} \quad (\text{S14})$$

Finally, by noticing $\text{Tr} [B^T H_V B] = \text{Tr} [H_V \kappa]$ and using the definitions of Λ^w and Λ , the right hand side is $e^{-V(x(\tau)) + V(x(0))} e^{h\tau\Lambda(\tau) - h\tau\Lambda^w(\tau)}$. Hence one arrives immediately at Eq. (6) of the main text.

B. Derivation using time-evolution operator

An alternative derivation of (6) is obtained by using a ‘tilted’ generator (or master operator) for the biased ensemble of trajectories. Let $u^h(x, \tau)$ be the (unnormalised) probability density at time τ , obtained as a marginal of the path distribution P_h . As discussed, for example, in Appendix A.2 of [S3], this distribution evolves in time according to a generalised Feynman-Kac formula as

$$\frac{\partial}{\partial \tau} u^h = L^h[u^h], \quad (\text{S15})$$

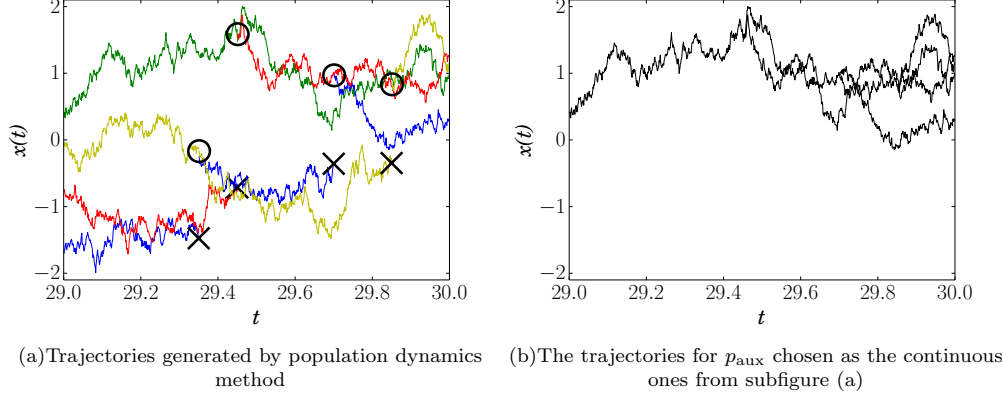


FIG. S2: (a) The trajectories generated by population dynamics method. We set $d = 1$, $A(x) = -x^3$, $B(x) = \sqrt{\epsilon}$, $\lambda(x) = x^2 + x$, and $h = \epsilon = 1$. The whole simulation time τ is 30, ΔT is set to be 0.05. The time step for solving the Langevin equation is 0.001. The number of copies N_c is 4. We mark \times when the trajectory is eliminated, and \circ when it is multiplied. (b) Time-reversed trajectories generated from (a): From the trajectories shown in (a), we follow the procedure described in Section IB, and generate (b).

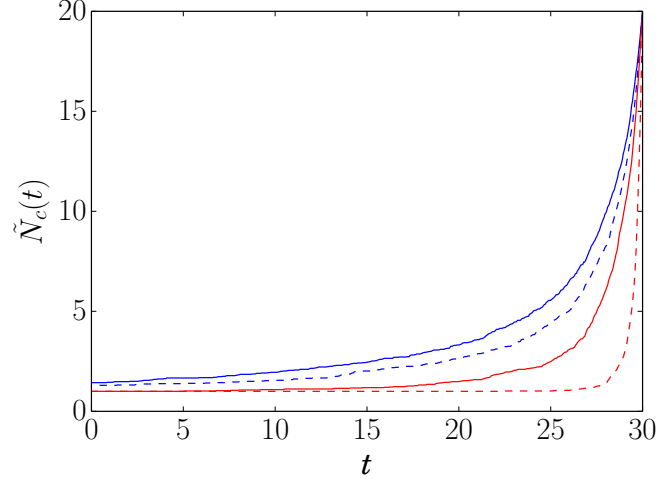


FIG. S3: The number of independent trajectories $\tilde{N}_c(t)$ obtained from the time-reversed method explained in Section IB for $h = -1$ (blue lines) and $h = 1$ (red lines). The line type corresponds to the value of thermal noise: $\epsilon = 1$ (solid line) and $\epsilon = 0.1$ (dashed line). We performed the population dynamics with $N_c = 20$, $\tau = 30$, and estimated the number of the trajectories $\tilde{N}_c(t)$. We repeat this measurement 60 times, and the result plotted on the figure is the average of those. We observe that $\tilde{N}_c(t)$ decreases very rapidly as t decreases to 0, especially for $h = 1$ with $\epsilon = 0.1$.

with

$$L^h[f] \equiv L_{\text{FP}}^F[f] + h(\lambda_d + \lambda_c \cdot F)f + \frac{h^2}{2}(\lambda_c \cdot \kappa \lambda_c)f - h\nabla \cdot (\kappa \lambda_c f). \quad (\text{S16})$$

Here, the Fokker-Planck operator L_{FP}^F is

$$L_{\text{FP}}^F[f] = -\nabla \cdot [Ff] + \frac{1}{2} \sum_{i,j} \frac{\partial^2}{\partial x_i \partial x_j} \kappa_{ij} f, \quad (\text{S17})$$

where the superscript F on L_{FP}^F indicates that the particle feels the physical force F introduced in the main text equation (1). Note that p_{end} is the eigenvector (normalised as probability) of the tilted Fokker-Planck operator L^h

associated to the eigenvalue $G(h)$: $L^h[p_{\text{end}}] = G(h)p_{\text{end}}$. The distribution p_{ave} is obtained from the eigenvector q of the tilted backward Fokker-Planck operator, defined as $(L^h)^\dagger[q] = G(h)q$, multiplied by p_{end} : one has $p_{\text{ave}} = q p_{\text{end}}$ [9].

Considering now the controlled population dynamics, the analogue of u^h is $u^w(x, \tau)$, which evolves as $\frac{\partial}{\partial \tau} u^w = L^w[u^w]$, with

$$L^w[f] \equiv L_{\text{FP}}^{F+w}[f] + h\lambda^w f. \quad (\text{S18})$$

The relation (6) of the main text follows from a duality relation between L^h and L^w . To be precise,

$$L^h[f] = e^V L^w[fe^{-V}]. \quad (\text{S19})$$

This relation may be verified directly from (S16,S18), noting that the potential V is related to the control w via the definition $w = h\kappa\lambda_c - \kappa\nabla V$. From (S15) we note that the operator $U_\tau^h = e^{\tau L^h}$ corresponds to integration forward in time over a duration τ . Similarly $U_\tau^w = e^{\tau L^w}$, and from (S19) we have $U_\tau^h[f] = e^V U_\tau^w[fe^{-V}]$. Setting $f(x) = \delta(x - x_0)$, then $u^h(x, \tau|x_0, 0) = U_\tau^h[f]$ is the (unnormalised) probability density at x , for a particle that was at x_0 a time τ earlier. Defining similarly $u^w(x, \tau|x_0, 0)$, (S19) implies

$$u^h(x, \tau|x_0, 0) = e^{V(x)} u^w(x, \tau|x_0, 0) e^{-V(x_0)}. \quad (\text{S20})$$

Hence one arrives at (6) of the main text.

This operator approach also allows to see why the control force w does not affect the intermediate-time distribution. One notes that $L^w[p_{\text{end}}^w] = G(h)p_{\text{end}}^w$ (the eigenvalue being $G(h)$ as seen from (S19)) and that $p_{\text{ave}}^w = q^w p_{\text{end}}^w$ where $(L^w)^\dagger[q^w] = G(h)q^w$. The relation (S19) also provides the connection between the controlled eigenvectors and the original ones at $w = 0$: one has $p_{\text{end}}^w = e^{-V} p_{\text{end}}$ and $q^w = e^V q$. This implies as announced in the main text that $p_{\text{ave}}^w = q^w p_{\text{end}}^w = p_{\text{ave}}$. The end-time distribution p_{end}^w is on the contrary affected by the control force w .

In the special case where w is given by the optimal control w^* (that is defined as the control w satisfying the condition $p_{\text{ave}}^w = p_{\text{end}}^w$ in the main text), one can show that the controlled system is described by the auxiliary process [S4] (or the “driven process” [S3]), which is a Markov process whose path probability density is equivalent to P_h in its stationary regime. (Indeed, $p_{\text{ave}}^w = p_{\text{end}}^{w^*}$ implies $q^{w^*} = 1$, which expresses that L^{w^*} conserves probability.) In this case one has [S3]

$$e^{-V} L^h[fe^V] = L_{\text{FP}}^{F+w^*}[f] + G(h)f, \quad (\text{S21})$$

where $G(h)$ is a constant (independent of x): this is the cumulant generating function. Comparing with (S19) one sees that $\lambda^{w^*}(x)$ is independent of x , from which it follows that the population dynamics in this case has no cloning or deletion of clones (this property is true for all finite N_c : all clones have equal weights at all times).

III. AN ALGORITHM FOR POPULATION DYNAMICS WITH A FEEDBACK CONTROL

Here, in order to complement the section *Iteration and feedback* in the main text, we explain the algorithm of the feedback population dynamics. As explained in the main text, the procedure is a combination of the population dynamics and an iterative measurement of the modifying potential $V(x)$.

1. Generate N_c initial conditions, for example, drawn from the stationary distribution of the original (unbiased) system. $V(x)$ is set to be 0 at the beginning.
2. Repeat the following feedback procedure R times. (r is the index representing how many times the procedure will be performed ($r = 0 \dots R - 1$)). (We denote by $V^r(x)$ the modifying potential $V(x)$ during the r -th loop. For example, $V^0(x) = 0$.)
 - (a) For a fixed time interval τ (which is sufficiently long compared with the correlation time of the observable $\lambda_{d,c}$), the population dynamics is performed as explained in section I. From the result, we obtain the trajectories $(x_a^V(t))_{a=0}^{N_c}$ ($t \in [0, \tau]$) and also the ones that have survived on $[0, \tau]$ $(y_a^V(t))_{a=1}^{\tilde{N}_c(t)}$ ($t \in [0, \tau]$) with their multiplicity $(k_a^V(t))_{a=1}^{\tilde{N}_c(t)}$ ($t \in [0, \tau]$), which are generated from the time-reversing method in section IB.
 - (b) Then, we start from the final condition of $x_a^V(t)$ and perform another population dynamics. This allows us to have again the trajectories $(x_a^V(t))_{a=0}^{N_c}$ ($t \in [\tau, 2\tau]$) and also the ones that have survived at time 2τ $(y_a^V(t))_{a=1}^{\tilde{N}_c(t)}$ ($t \in [\tau, 2\tau]$) with multiplicity $(k_a^V(t))_{a=1}^{\tilde{N}_c(t)}$ ($t \in [\tau, 2\tau]$).

(c) Repeat this procedure M times. We finally have trajectories $(x_a^V(t))_{a=0}^{N_c}$ ($t \in [0, M\tau]$) and also the trajectories $(y_a^V(t))_{a=1}^{\tilde{N}_c(t)}$ ($t \in [0, M\tau]$) with their multiplicity $(k_a^V(t))_{a=1}^{\tilde{N}_c(t)}$ ($t \in [0, M\tau]$).

(d) From these trajectories, we evaluate $p_{\text{end}}^w(x)$ and $p_{\text{ave}}^w(x)$ by

$$p_{\text{end}}^w(x) \sim \frac{1}{M\tau N_c} \sum_{a=1}^{N_c} \int_0^{M\tau} \delta(x_a^V(t) - x) dt. \quad (\text{S22})$$

$$p_{\text{ave}}^w(x) \sim \frac{1}{M(\tau - t_{\text{end}}) N_c} \sum_{m=0}^{M-1} \int_{m\tau}^{(m+1)\tau - t_{\text{end}}} \sum_{a=1}^{\tilde{N}_c(t)} k_a^V(t) \delta(y_a^V(t) - x) dt. \quad (\text{S23})$$

The reason why, in $p_{\text{ave}}^w(x)$, we set the upper bound of integration to $(r+1)\tau - t_{\text{end}}$ is to avoid a transient regime: By setting t_{end} to be much larger than a correlation time, one can make the statistics of the result to be better. (We note that if τ is sufficiently large, this setting is not necessary.)

(e) Finally, from these distribution functions, $V^{r+1}(x)$ is given as [10]

$$V^{r+1}(x) = V^r(x) - [\log p_{\text{ave}}^w(x) - \log p_{\text{end}}^w(x)], \quad (\text{S24})$$

which corresponds to (7) in the main text.

3. Go to the next loop of r with the new modifying potential $V^{r+1}(x)$. The initial condition is set to be the final value of $x_a^V(M\tau)$ in the previous population dynamics method.

We note that the first loop of the feedback (loop $r = 0$) corresponds to the normal population dynamics method. As the number of the repetition with respect to r becomes larger, the control potential V gets close to its optimal control form.

IV. LANGEVIN SYSTEM WITH QUARTIC POTENTIAL

In this final section, in order to complement the sections *Numerical example* and *Outlook* in the main text, we explain the property of the system we considered there: the parameters are given by $d = 1$, $F(x) = -x^3$, $B(x) = \sqrt{2\epsilon}$, $\lambda_d(x) = \lambda(x) \equiv x + x^2$ and $\lambda_c(x) = 0$. We focus on the small-noise limit $\epsilon \rightarrow 0$. Throughout this section, h corresponds to \bar{h} in the main text (see below).

The main features of the limit $\epsilon \rightarrow 0$ are

- The distribution $p_{\text{ave}}(x)$ concentrates on a point x_{ave} that is a root of the polynomial

$$3x^5 - 4hx - 2h = 0.$$

This function is sketched in Fig. S4. For $h > 0$, the concentration is at the positive root ($x_{\text{ave}} > 0$); for $h = 0$ one has $x_{\text{ave}} = 0$. For negative h , the point x_{ave} decreases quickly from zero and localises at $x_{\text{ave}} \approx \frac{1}{2}$.

- There is a second-order dynamical phase transition at $h = 0$, which appears as divergence of the second derivative of the dynamical free energy, $G''(h)$ (see Fig. S5, below).
- The distribution $p_{\text{end}}(x)$ concentrates on a point x_{end} , with $x_{\text{end}} \neq x_{\text{ave}}$ in general. This leads to poor convergence of the population dynamics method for small ϵ , as discussed in the main text.
- Even though the system is simple, the analytical expressions of p_{ave} and p_{end} are not straightforward. In particular, the perfect potential $V^*(x)$ corresponding to $w^*(x)$ is not expressed exactly as the quartic polynomial expansion used to perform a numerical evaluation of $w(x)$ – however, as described in the main text, this does not affect the effectiveness of the numerical procedure.

Below, relying on the Euler-Lagrange equation, we derive the analytical results of $G(h)$, p_{ave} and p_{end} in $\epsilon \rightarrow 0$, from which these features are obtained.

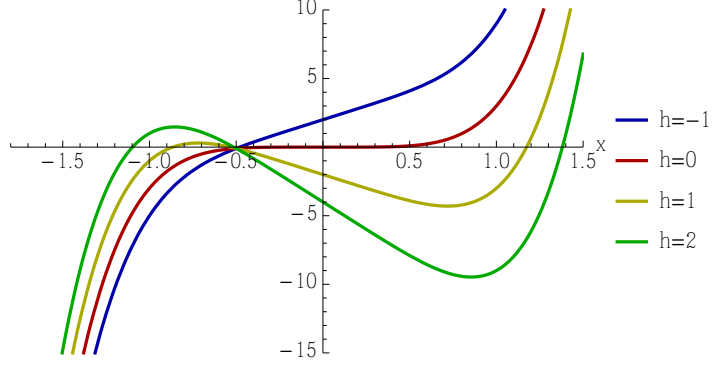


FIG. S4: Plots of the polynomial $3x^5 - 4hx - 2h$ for several h . The roots of this polynomial determine the concentration points of $p_{\text{ave}}(x)$ for $\epsilon \rightarrow 0$ in the model system considered below.

A. Euler-Lagrange equation (Instanton equation)

We consider the following finite time cumulant generating function:

$$G_{\tau,\epsilon}(h) = \frac{\epsilon}{\tau} \log \left\langle e^{(\tau/\epsilon)h\Lambda(\tau)} \right\rangle_{\text{st}}, \quad (\text{S25})$$

where $\langle \rangle_{\text{st}}$ means the average with respect to the path with a stationary initial condition. (Hereafter, we denote this initial distribution function by $P_{\text{st}}(x)$.) The function $G_\epsilon(h) \equiv \lim_{\tau \rightarrow \infty} G_{\tau,\epsilon}(h)$ corresponds to $\tilde{G}(\tilde{h})$ in the main text. By taking $\epsilon \rightarrow 0$, we obtain the following variational principle:

$$\lim_{\epsilon \rightarrow 0} G_{\tau,\epsilon}(h) = -\frac{1}{\tau} \min_{x_0, x_\tau} \left[\min_{\substack{(x(t))_{t=0}^\tau \\ x(0)=x_0, x(\tau)=x_\tau}} \int_0^\tau L(\dot{x}(t), x(t)) dt + F_{\text{free}}(x_0) \right], \quad (\text{S26})$$

with the Lagrangian $L(\dot{x}, x)$ defined as

$$L(\dot{x}, x) \equiv \frac{1}{4} (\dot{x} - F(x))^2 - h\lambda(x), \quad (\text{S27})$$

and also the free energy function $F_{\text{free}}(x_0)$ defined as

$$F_{\text{free}}(x_0) \equiv -\lim_{\epsilon \rightarrow 0} \epsilon \log P_{\text{st}}(x_0) = \frac{1}{4} x_0^4 + \text{const.} \quad (\text{S28})$$

Then, the corresponding Euler-Lagrange equation (Hamilton equation), which is obtained from minimising this action, is

$$\dot{x} = -x^3 + 2p \quad (\text{S29})$$

$$\dot{p} = 3px^2 - h(2x + 1), \quad (\text{S30})$$

with the required initial and the final conditions as

$$p(0) = \frac{\partial F_{\text{free}}(x)}{\partial x} \Big|_{t=0} = x(0)^3 \quad (\text{S31})$$

$$p(\tau) = 0. \quad (\text{S32})$$

We analyse these equations numerically and analytically in [S5]. The following results are based on that study.

B. Steady solutions

Here, we consider the steady solutions of these instantons, which is defined as the solution obtained from $\dot{x}_{\text{st}} = \dot{p}_{\text{st}} = 0$ in (S29) and (S30). These conditions lead to

$$p_{\text{st}} = \frac{1}{2}x_{\text{st}}^3 \quad (\text{S33})$$

and

$$3x_{\text{st}}^5 - 4hx_{\text{st}} - 2h = 0. \quad (\text{S34})$$

We plot the left-hand side of (S34) as a function of x in Fig.S4 for several fixed h . The figure shows that this equation has three solutions, when h is larger than a certain value (larger than 0).

C. Cumulant generating function

From the variational principle (S26), even in the case where there are multiple instanton solutions, the cumulant generating function can be calculated. This is based on the observation that the instanton solution corresponding to the minimum is time-independent [11]. More precisely, by combining this observation with the variational principle (S26), we get

$$\lim_{\epsilon \rightarrow 0} G_\epsilon(h) = \max_{x_{\text{st}}} G_{\text{st}}(x_{\text{st}}), \quad (\text{S35})$$

with

$$G_{\text{st}}(x_{\text{st}}) \equiv -\frac{1}{4}x_{\text{st}}^6 + h(x_{\text{st}}^2 + x_{\text{st}}). \quad (\text{S36})$$

We plot the $\epsilon \rightarrow 0$ result, $\lim_{\epsilon \rightarrow 0} G_\epsilon(h)$, in Fig.S5, from which we can see that the generating function has a kink at the origin, which is the sign of the dynamical phase transition in this system, appearing in the zero-temperature limit [12].

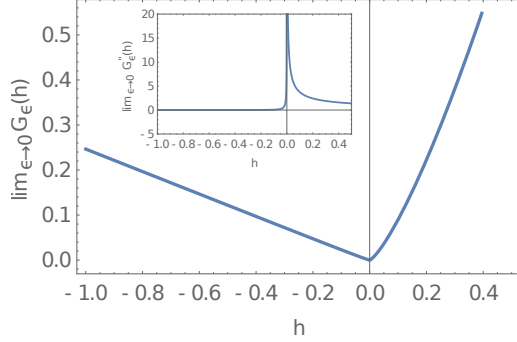


FIG. S5: Generating function $\lim_{\epsilon \rightarrow 0} G_\epsilon(h)$ as a function of h , as obtained from (S35-S36). We can see that there is a singularity at $h = 0$ representing a second-order dynamical phase transition, as illustrated on the inset by the divergence in $h = 0$ of the second derivative.

D. Analytical expressions of $p_{\text{end}}(x)$ and $p_{\text{ave}}(x)$ in $\epsilon \rightarrow 0$

Finally, we write the explicit analytical expressions of $p_{\text{end}}(x)$ and $p_{\text{ave}}(x)$ in the $\epsilon \rightarrow 0$ limit. We consider the biased (unnormalised) probability density u^h introduced in the beginning of Section II B. We also consider the same function but with fixed initial condition $u^h(x, \tau|x_0, \tau)$. By using these function, we introduced two logarithmic functions defined as

$$W_F(x, t) \equiv \epsilon \log u^h(x, t), \quad (\text{S37})$$

$$W_B(x, t) \equiv \epsilon \log \int u^h(y, t|x, 0) dy. \quad (S38)$$

From the generalised Feynman-Kac formula (S15), we obtain the time evolution equation for them as

$$\frac{\partial}{\partial t} W_F(x, t) = -\epsilon \frac{\partial}{\partial x} F(x) - F(x) \frac{\partial}{\partial x} W_F(x, t) + \epsilon \left(\frac{\partial}{\partial x} \right)^2 W_F(x, t) + \left(\frac{\partial}{\partial x} W_F(x, t) \right)^2 + h \lambda(x). \quad (S39)$$

and

$$\frac{\partial}{\partial t} W_B(x, t) = F(x) \frac{\partial}{\partial x} W_B(x, t) + \epsilon \left(\frac{\partial}{\partial x} \right)^2 W_B(x, t) + \left(\frac{\partial}{\partial x} W_B(x, t) \right)^2 + h \lambda(x). \quad (S40)$$

These equations can be solved in $\epsilon = 0$ with t large asymptotics. Indeed, by setting $W_F(x, t) = tG(h) + W_F(x)$ and $W_B(x, \tau - t) = (\tau - t)G(h) + W_B(x)$ with $G(h) \equiv \lim_{\epsilon \rightarrow 0} G_\epsilon(h)$ in these expressions, we obtain the equations to determine $W_F(x)$ and $W_B(x)$ as

$$\frac{\partial W_F(x)}{\partial x} = \frac{1}{2} \left[F(x) + C_h(x) \sqrt{F(x)^2 - 4h\lambda(x) - \min_y [F(y)^2 - 4h\lambda(y)]} \right], \quad (S41)$$

and

$$\frac{\partial W_B(x)}{\partial x} = \frac{1}{2} \left[-F(x) + C_h(x) \sqrt{F(x)^2 - 4h\lambda(x) - \min_y [F(y)^2 - 4h\lambda(y)]} \right]. \quad (S42)$$

with

$$C_h(x) = 1 \quad (x < x_{\min}), \quad (S43)$$

$$C_h(x) = -1 \quad (x > x_{\min}), \quad (S44)$$

where

$$x_{\min} \equiv \text{Argmin}_x [F(x)^2 - 4h\lambda(x)]. \quad (S45)$$

Equations (S41) and (S42) are the key result in this subsection. From them, we indeed get

$$p_{\text{end}}(x) \sim \exp \left[(1/\epsilon) \int^x \frac{1}{2} \left[F(y) + C_h(y) \sqrt{F(y)^2 - 4h\lambda(y) - \min_z [F(z)^2 - 4h\lambda(z)]} \right] dy \right] \quad (S46)$$

and

$$p_{\text{ave}}(x) \sim \exp \left[(1/\epsilon) \int^x C_h(y) \sqrt{F(y)^2 - 4h\lambda(y) - \min_z [F(z)^2 - 4h\lambda(z)]} dy \right]. \quad (S47)$$

Also from the same equations, we get the most probable x in $p_{\text{end}}(x)$ and $p_{\text{ave}}(x)$ with $\epsilon \rightarrow 0$. We denote them by x_{end} and x_{ave} , respectively. Then, from (S46) and (S47), we find that these values satisfy

$$x_{\text{ave}} = \text{Argmax}_{x_{\text{st}}} G_{\text{st}}(x_{\text{st}}) \quad (S48)$$

where $G_{\text{st}}(h)$ is defined in (S35), and

$$\frac{F(x_{\text{ave}})^2}{4h} = \lambda(x_{\text{ave}}) - \lambda(x_{\text{end}}). \quad (S49)$$

Since $\frac{F(x_{\text{ave}})^2}{4h} \neq 0$, x_{ave} and x_{end} are different from each other. In other words, p_{ave} and p_{end} concentrate on different values of their argument in the $\epsilon \rightarrow \infty$ limit, as announced in the main text.

For checking the validity of the obtained expressions, we numerically solve the equations (S39) and (S40) during a sufficiently large time interval t . We set $h = 1$ (Fig.S6(a) and Fig.S6(c)) and $h = -1$ (Fig.S6(b) and Fig.S6(d)). The different colours represent the different values of ϵ : yellow, blue, red lines correspond to $\epsilon = 1, 0.5, 0.1$, respectively. In the same figure, we plot the analytical lines (S41) and (S42), with $C_h = 1$ (for all x) (black solid line) and $C_h = -1$

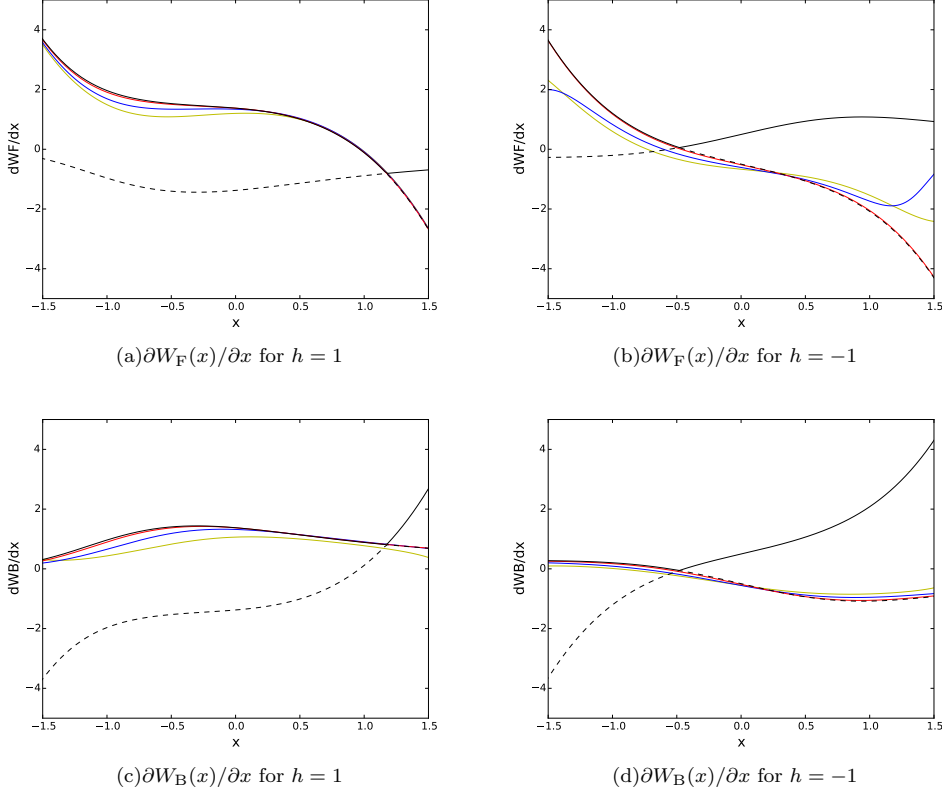


FIG. S6: The functions $\partial W_F(x, t)/\partial x$ and $\partial W_B(x, t)/\partial x$ obtained in the large t limit by solving numerically (S39) and (S40) [coloured solid lines]. We set $h = 1$ ((a) and (c)) and $h = -1$ ((b) and (d)). The colours correspond different values of ϵ : yellow, blue and red lines correspond to $\epsilon = 1, 0.5, 0.1$, respectively. To illustrate the determination of the \pm sign of C_h in the analytical results (S41) and (S42), we also plot on each subfigure those results with the choice of $C_h = 1$ (for all x) as black solid lines and the choice of $C_h = -1$ (for all x) as black dashed lines. As the noise goes to zero, we observe the convergence of the functions $\partial W_F(x, t)/\partial x$ and $\partial W_B(x, t)/\partial x$ determined numerically at large t towards the analytical line (S41) and (S42), where the $+$ sign in \pm is taken for $x < x_{\min}$ and the $-$ sign is taken for $x > x_{\min}$.

(for all x) (black dashed line). We can see the convergence of the numerical lines (with decreasing ϵ) towards the analytical lines (S41) and (S42), where $+$ sign is chosen for $x < x_{\min}$ and $-$ sign is chosen for $x > x_{\min}$.

[S1] J. Tailleur, V. Lecomte, AIP Conf. Proc., Vol 1091, pp. 212-219 (2009) MODELING AND SIMULATION OF NEW MATERIALS: Proceedings of Modeling and Simulation of New Materials: Tenth Granada Lectures.

[S2] H. Touchette, Phys. Rep. **478**, 1, (2009).

[S3] R. Chetrite and H. Touchette, Ann. Henri Poincaré **16**, 2005 (2015)

[S4] R. L. Jack and P. Sollich, Prog. Theor. Phys. Suppl. **184**, 304 (2010).

[S5] In preparation by T. Nemoto and F. Bouchet.

[S6] C. Giardinà, J. Kurchan, and L. Peliti, Phys. Rev. Lett. **96**, 120603 (2006).

[7] This quantity would represent the exponential growth rate of the system if population had not been kept constant.

[8] A property of the empirical distribution for the sample paths, taken at a fixed time t_0 , is that it is independent of t_0 as long as this intermediate time is taken far enough from initial and final transient regimes; this is fully justified in the footnote [9].

[9] See for example [S6]. The essence of the derivation is as follows: The distribution $p_{\text{ave}}(x_1)$ measures the density of x_1 at an intermediate time t_0 far from the initial time and from the final time τ . To relate it to the spectral elements of L^h , consider the time-evolution operator $U_\tau^h = e^{\tau L^h}$. Defining $f_0(x) \equiv \delta(x - x_0)$, $f_1(x) \equiv \delta(x - x_1)$, one has that the function (of x_1, x_0) defined as $\int U_{\tau-t_0}^h [f_1 U_{t_0}^h [f_0]] dx$ ($= U_{t_0}^h [f_0] (x_1) \int U_{\tau-t_0}^h [f_1] dx$) is proportional to $p_{\text{ave}}(x_1)$ in the limit $t_0 \rightarrow \infty$

and $\tau - t_0 \rightarrow \infty$. The right eigenvector of L_h associated to $G(h)$ is p_{end} and one denotes by q its left eigenvector (which is also the right eigenvector of $(L^h)^\dagger$). The large-time behaviour of the evolution operator is $U_\tau^h[f_0] \sim q(x_0)p_{\text{end}}(x_0)e^{\tau G(h)}$. Then $p_{\text{ave}}(x_1) \propto q(x_0)p_{\text{end}}(x_1) \int q(x_1)p_{\text{end}}(x)dx \propto q(x_1)p_{\text{end}}(x_1)$ as announced. We note that the result does not depend on the intermediate time t_0 , as long as t_0 is far enough from the initial and final times. This justifies the expression (S8) used to evaluate p_{ave} numerically.

- [10] For a better convergence, we sometimes use the update equation as $V^{r+1}(x) = V^r(x)(1 - \alpha) + \{V^r(x) - 2\epsilon [\log p_{\text{ave}}^w(x) - \log p_{\text{end}}^w(x)]\} \alpha$, with an arbitrary parameter α ($\alpha = 0 \sim 1$). Also, for the practical way to obtain the distribution function $p_{\text{end,ave}}(x)$, we use an effective description. See the next subsubsection.
- [11] We can prove this fact from a linear stability analysis. See [S5] for the detail.
- [12] One can numerically check that the transition is first-order, by showing divergence in the second derivative, with keeping the continuity in the first derivative.